SAR for Archaeological Prospection in Europe and in the Middle East

Christopher Stewart

Abstract This chapter describes recent studies on the use of synthetic aperture radar for archaeological prospection and anthropogenic feature extraction. Radar remote sensing can provide unique information about objects on the ground from its sensitivity to the relative permittivity of materials and to surface roughness, as a function of the microwave wavelength. Methods have been developed to detect residues of buried structures over land cover types typical to Europe and the Middle East. These include agriculture, grassland and sand-covered areas. The techniques attempt to exploit the full information content of radar data, contained in both the amplitude and phase of the signal. They also attempt to make efficient use of time series. Results show that surface residues of buried archaeological structures in temperate vegetated areas can be identified in variously processed radar images. Anthropogenic features in sand-covered areas can also be efficiently detected. Developments in Big Data analytics and Earth observation data accessibility have the potential to bring radar remote sensing closer to the cultural heritage community.

Keywords Synthetic Aperture Radar · Big Data · Cultural Heritage · Archaeological Prospection

Introduction

Microwave signals emitted by active sensors are uniquely sensitive to various properties of target materials. Synthetic aperture radar (SAR) imagery can reveal subtle variations in surface roughness, relative to the signal wavelength (Ulaby et al. 1982). SAR is also sensitive to the relative permittivity of materials (Massonnet and Souyris 2008), which, in the case of soils, is largely related to the presence of moisture (Dubois et al. 1995). Variations in surface roughness and moisture content may

C. Stewart (✉)
Earth Observation Programmes, Future Systems Department, European Space Agency (ESA), Frascati, Italy

D. G. Hadjimitsis et al. (eds.), *Remote Sensing for Archaeology and Cultural Landscapes*, Springer Remote Sensing/Photogrammetry,
https://doi.org/10.1007/978-3-030-10979-0_5

indicate the presence of archaeological objects (Wiseman and El-Baz 2007; Stewart 2017). Moreover, in dry sand, the low relative permittivity may permit some signal penetration, which can also be exploited for archaeological applications (Stewart et al. 2016).

Despite the utility of SAR for archaeological applications, microwave remote sensing has experienced a slower rate of uptake by the cultural heritage community than remote sensing in the optical region. This is perhaps due to the challenges associated with the processing and interpretation of radar data and, until recently, high costs and lack of data availability.

We are currently experiencing an unprecedented increase in the volume, variety and velocity of remote data acquisition, referred to as "Big Data" (Manyika et al. 2011). Moreover, we are seeing a positive trend in the availability, accessibility and openness of scientific data and results. These developments are revolutionising the way remote sensing is carried out and is opening up opportunities for users of existing and new application areas, including cultural heritage.

This chapter summarises recent studies that aim to take advantage of new opportunities brought by the Big Data revolution to exploit large time series of SAR data for archaeological prospection. Two studies are described here. Each focuses on very different geographical regions, land cover types and methods of prospection. The first involves the use of SAR to detect vegetation or soil residues of buried archaeological structures in areas surrounding the city of Rome, in Italy. The second demonstrates the use of SAR to efficiently detect buried or surface traces of human activity in sand-covered regions of North Sinai, Egypt.

SAR in Vegetated Areas

The aim of the study presented here is to assess the use of both the amplitude and phase of the SAR signal to detect surface residues of buried archaeological structures in a temperate vegetated region. These are likely to be indirect indicators of buried structures in the form of crop or soil marks. No significant penetration of the radar signal into the ground would take place in these areas given the high relative permittivity from the water in the soil and the overlying vegetation. The research summarised here is described in more detail in Stewart (2017).

Six areas of interest (AOIs) have been selected for the analysis. These all surround the area of Rome and comprise agricultural fields or pasture beneath which archaeological structures are known to exist from noninvasive archaeological survey (see Fig. 1). The geology of three of the AOIs (Appia, Prenestina and Veii) is characterised by volcanic deposits, mainly pyroclastic tuff, from the Albano and Sabatino volcano districts, with undulating eroded valleys. The remaining three AOIs of Ostia, Portus and Salaria are in the alluvial Tiber valley and delta, characterised by very flat topography.

The SAR data procured for the analysis includes a large time series of very-high-resolution imagery acquired by the Italian Constellation of Small Satellites for

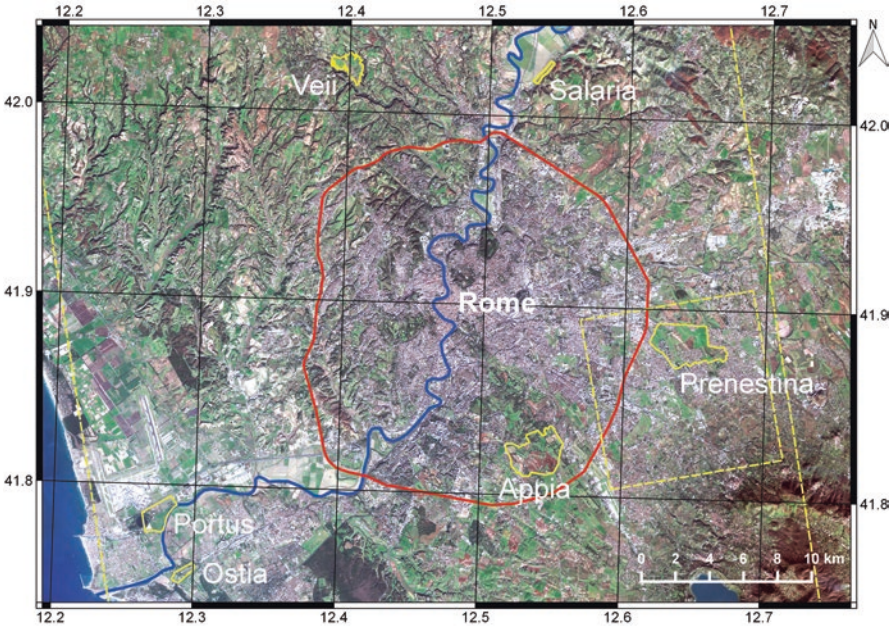

Fig. 1 Areas of interest (AOIs) shown in yellow polygons. Footprints of CSK stripmap and spotlight data shown as dashed yellow rectangles

Table 1 Details of CSK data acquired for the analysis

Sensor mode	Enhanced spotlight	Stripmap HIMAGE
Number of scenes	27	77
Acquisition date range (year/month)	2010/06 to 2012/08	2011/03 to 2015/07
Polarisation	24 × HH, 3 × VV	HH
Pass	Asc	Asc
Scene centre incidence angle	25.25	33.95
Spatial resolution	1 m	2.5 m
Wavelength	3.1 cm (X-band)	

Mediterranean basin Observation (COSMO-SkyMed) (see Table 1). This data was provided by the Italian Space Agency (ASI). It was obtained for the following reasons: (1) to have as large as possible a time series in order to cover a range of environmental and ground conditions; (2) to have data at the highest available spatial resolution, to resolve small-scale features corresponding to recognisable archaeological structures; and (3) to have the highest possible frequency of acquisition, to be able to perform coherence and interferometric SAR (InSAR) digital elevation model (DEM) calculation, without complete loss of coherence.

Processing was carried out to derive three types of information from the SAR data, including (1) multitemporal speckle filtered backscatter, which may be sensi-

tive to roughness and moisture anomalies at the surface caused by underlying archaeological structures; (2) interferometric coherence, which may be sensitive to small-scale random change between acquisitions, which in turn may provide an indicator of vegetation characteristics altered by the presence of buried structures; and (3) DEM, derived from interferometry, to detect subtle surface topographic traces of archaeological features beneath the ground.

Filtered Backscatter (Roughness and Moisture Anomalies)

As previously stated, SAR backscatter is sensitive to variations in both surface roughness and soil moisture content. Subtle changes in either may be due to the presence of buried structures, which may result from the same mechanisms which lead to the well-studied phenomena of crop and soil marks (Jones and Evans 1975; Evans and Jones 1977; Wilson 2000; Agapiou et al. 2013). These may be visible as differences in SAR backscatter. To better distinguish these from the image speckle, a method was adopted to remove as much of the image speckle as possible while retaining the spatial resolution and small differences which may appear in individual images. To achieve this, multitemporal De Grandi (1997), speckle filtering was carried out. The De Grandi filter averages in the temporal domain parts of images that are statistically homogenous, reducing the speckle, but retaining key statistical backscatter properties of each single image. If an area of the coregistered images contains a feature in only one or a few images, the areas to be averaged are divided to exclude this feature (De Grandi et al. 1997). The De Grandi filter preserves the spatial resolution of the input images. The De Grandi filter is thus suitable for identifying small anomaly features with only slight variations in backscatter from surrounding areas (De Grandi et al. 1997; Stewart et al. 2016).

Interferometric Coherence (Small-Scale Random Change Between Acquisitions as Indicator of Vegetation Characteristics)

Another type of information that was extracted from the SAR data for the analysis includes the interferometric coherence between consecutive CSK image acquisitions. The interferometric coherence can provide an indication of the extent of random and small-scale spatial change in surface materials between image acquisitions. Such change may include the position and orientation of plants as they are blown by the wind. This in turn may provide information on vegetation type and growth, as the extent of random wind-driven displacement differs by vegetation type and stage of growth. Subtle differences in vegetation type and height may be due to underlying archaeological structures.

DEM (Subtle Surface Relief Variations)

A third type of information includes heights calculated through SAR interferometry (InSAR). Given the right conditions, with InSAR it is possible to derive height information through the phase difference between SAR image acquisitions separated by a spatial baseline perpendicular to the satellite azimuth. To derive such information over mainly vegetated areas, it was necessary to apply a technique called SBAS (small baseline subsets) (Berardino et al. 2002). SBAS works through the generation of many interferograms, each with minimal spatial (for displacement velocities) and temporal baselines between acquisitions to avoid decorrelation effects (Berardino et al. 2002). SBAS is mainly used to calculate small-scale displacement, but it can also be used for DEM generation.

Analysis of Features

Surface residues of buried structures have been found in the filtered CSK backscatter, coherences and DEMs. In an attempt to understand the mechanisms and conditions responsible for the appearance of residues in each layer in which they were present, an analysis of results has been carried out with interferometric coherence (calculated from the SAR data) and potential soil moisture deficit (PSMD) (derived from rainfall and potential evapotranspiration measurements). The methodology is described in more detail in Stewart (2017).

Results

Archaeological residues were found in all three types of processed SAR data (backscatter, coherence and DEM). More residues were found in the area of the Tiber valley and delta, characterised by alluvial substrate and flat topography. Less residues were found in the volcanic districts on either side of the Tiber valley, characterised by a volcanic substrate and undulating topography. Residues were found in particular in three of the AOIs (Portus, Salaria and Prenestina). In these areas, features in the processed SAR data corresponded with archaeological finds documented in the archaeological surveys. These are discussed here according to the type of SAR processed data on which they appeared.

Filtered Backscatter

De Grandi speckle filtering made a huge difference in the ability to detect potential archaeological features. Figure 2 shows the difference that De Grandi filtering can make on the clarity of features.

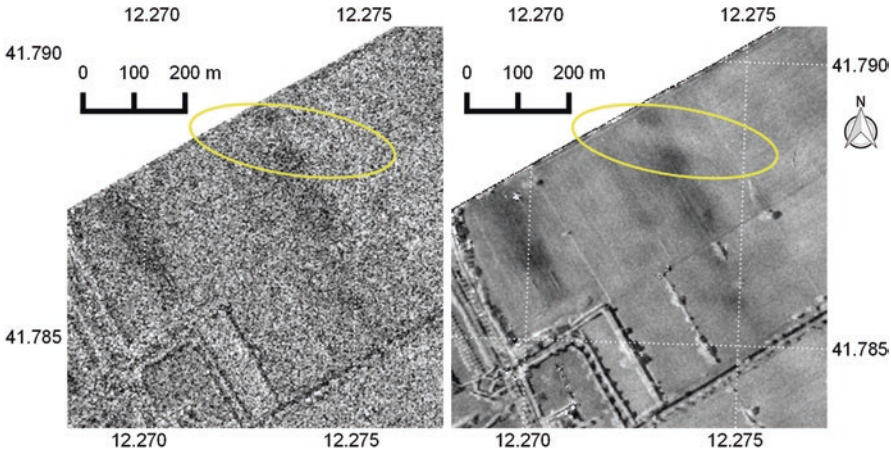

Fig. 2 Example of De Grandi multitemporal speckle filter. Left: Single image with surface residue of a buried Claudian canal (in yellow ellipse), barely evident in the Portus AOI. Right: The same image after having undergone De Grandi multitemporal speckle filtering using all 77 images in time series. The residue of the Claudian canal appears much clearer on the De Grandi filtered image

Several features of both high and low relative backscatter corresponded with buried archaeological structures in the Portus, Prenestina and Salaria AOIs.

In the Portus AOI, a feature of lower backscatter corresponds with built-up areas detected by a magnetometry survey carried out by Keay et al. (2005) (see Fig. 3). In the same AOI, a feature of higher backscatter corresponds with a Claudian canal, detected in the same survey (see Fig. 4). The two features are not correlated, in that they are not always visible in the same filtered imagery. Neither corresponds with PSMD.

The Claudian canal is more visible in times of high coherence (see Figs 4 and 6). At X-band wavelengths and 16-day temporal baselines, coherence is almost immediately lost (Zalite et al. 2016; Zalite et al. 2014). If coherence is high, it is likely therefore that the field is fallow or that it contains vegetation that does not move very much in the wind (such as beans tied to poles). In either case, it is likely that the feature is a soil mark.

The urban feature never appears clearly at times of high coherence (see Fig. 4). It is therefore possible that this is a crop mark, as vegetation tends to cause loss in coherence. The fact that the mark is distinguishable by lower backscatter would suggest the surface is less moist, or smoother; this would correspond with a negative crop mark, characterised by stunted growth caused by buried building material.

A feature of high backscatter was observed in some of the filtered backscatter imagery in the Prenestina AOI (see Figs 7 and 8). The feature corresponds with the suspected continuation of a buried road, documented by Quilici (1974). This may be a crop mark, given that the area is always characterised by low coherence.

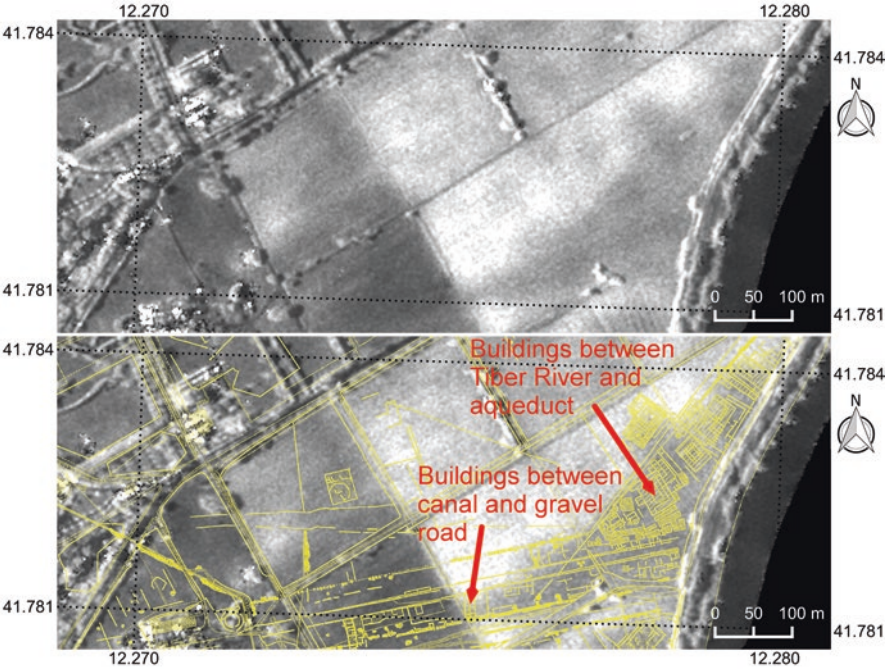

Fig. 3 Residue of buried buildings on image of De Grandi speckle filtered backscatter acquired on 9 July 2012. Overlain in yellow on the image below is the interpretation by Keay and his colleagues of the integrated archaeological survey (mainly magnetometry) published in Keay et al. (2005). COSMO-SkyMed data provided by the Italian Space Agency

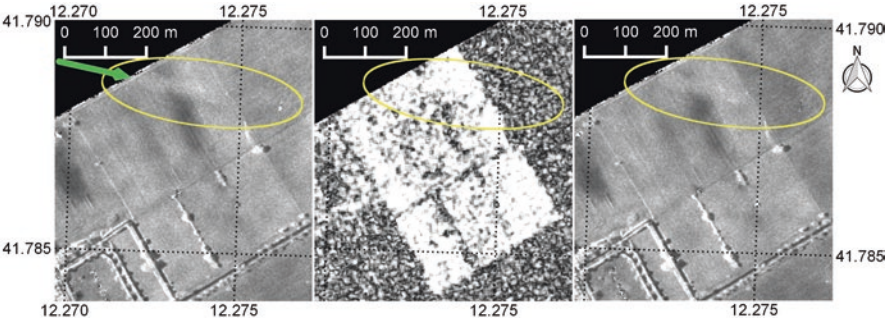

Fig. 4 Residue of Claudian canal (highlighted by yellow ellipse) on image of filtered backscatter acquired on 22 April 2011 (left) and 8 May 2011 (right). In the centre is the coherence image between these two acquisitions. Very-high coherence can be observed over the fields in which the residue is visible. The green arrow indicates the location and direction from which the photo in Fig. 5 was acquired. COSMO-SkyMed data provided by the Italian Space Agency

Fig. 5 Photo acquired of the location of the residue of the Claudian canal. Photo acquired on 24 May 2013 at 18:45. No trace of the Claudian canal is visible on the ground at the time of photo acquisition

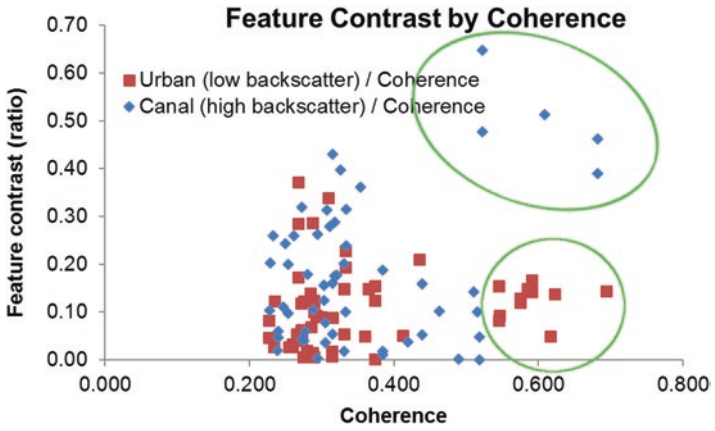

Fig. 6 Graph showing feature contrast (clarity) of the Claudian canal (in blue diamonds) and the urban area (in red squares), plotted against coherence. Where high coherence is observed, the contrast of the Claudian canal is often high, while the contrast of the urban area is consistently low. These patterns are shown in green ellipses

Moreover, it may be a positive crop mark, given that the feature is characterised by higher backscatter, due either to higher moisture or roughness, which may be a result of more abundant vegetation. The time of greatest feature visibility corresponds with highest PSMD. This would support the argument of a crop mark, which

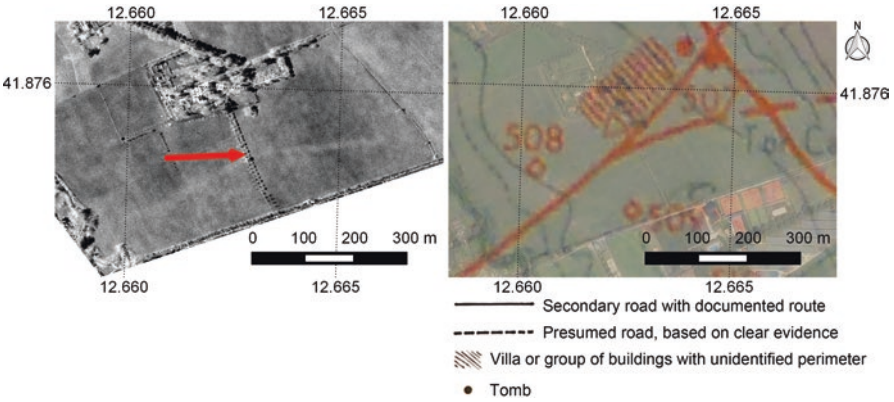

Fig. 7 Left: Residue of road visible on image of filtered backscatter, acquired on 25 July 2010. Right: Archaeological chart of Quilici (1974) of the same area overlain on true-colour Pleiades image acquired on 20 April 2014. Red arrow indicates location and direction from which photo in Fig. 8 was acquired. COSMO-SkyMed data provided by the Italian Space Agency. Pleiades data provided by the European Space Agency

Fig. 8 Photo of residue shown in Fig. 7, acquired on 19 September 2015 at 17:03. No evidence of residue was visible on the ground at that time

is more likely to appear at times of low moisture. No residues were found over the other features documented in this area. However, in most cases these have been interpreted from scant surface fragments which do not have a coherent form and are unlikely to leave a recognisable trace in the SAR data.

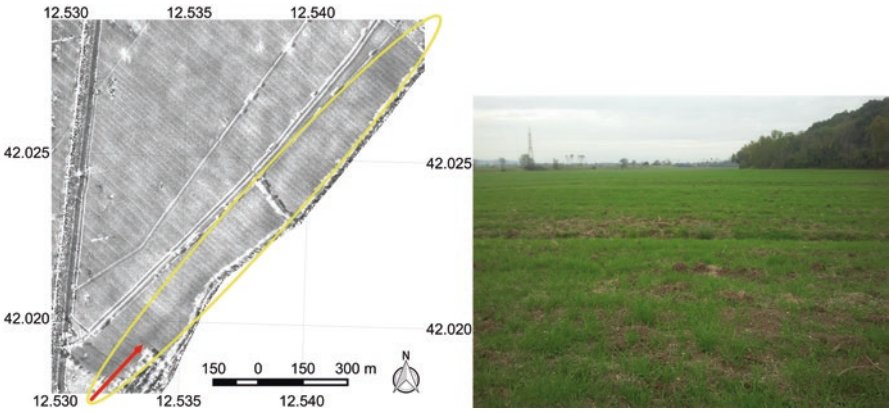

Fig. 9 Left: Image of filtered backscatter acquired on 7 April 2013 showing a trace of the ancient Via Salaria (highlighted by yellow ellipse). Red arrow indicates location and direction from which photo was acquired. Right: Photo acquired on 1 October 2016 at 17.14 of the location of the trace of the ancient Via Salaria. There was no visible evidence of the ancient Via Salaria on the ground at this time. COSMO-SkyMed data provided by the Italian Space Agency

In the Salaria AOI, a trace of the ancient Via Salaria is visible in some of the imagery (see Fig. 9). This appears as low backscatter. There is no clear correspondence between the feature clarity and PSMD, although the times of highest contrast coincide with a period of low PSMD, which is not a characteristic of crop marks. Throughout most of the time series, there is no clear feature contrast, and coherence is consistently low. At the time of feature contrast, the coherence is at the same low value as throughout most of the time period. Given that the feature is characterised by low backscatter, and given the low coherence in all images, it is likely that these residues are manifestations of negative crop marks. This would be possible if the paving stones of the ancient Via Salaria were buried beneath the ground.

Interferometric Coherence

In some cases, residues were present in the coherence images. These residues only occur over the Prenestina AOI and are always characterised by lower coherence. The residues correspond with the location of ancient roads documented by Quilici (1974). An inspection of these areas on the ground showed that most correspond with slight topographic valleys, although in one case no topography was visible on the ground. However, in this last case, a very-high-resolution DEM was produced from UAV photogrammetry in which a very slight topographic trace was notable. It may be therefore that the low coherence features are due to increased crop growth at the bottom of valleys where water would collect. The coherence residues generally appear at times of high soil moisture deficit and less with high soil moisture surplus. This also supports the argument that the coherence residues are crop marks.

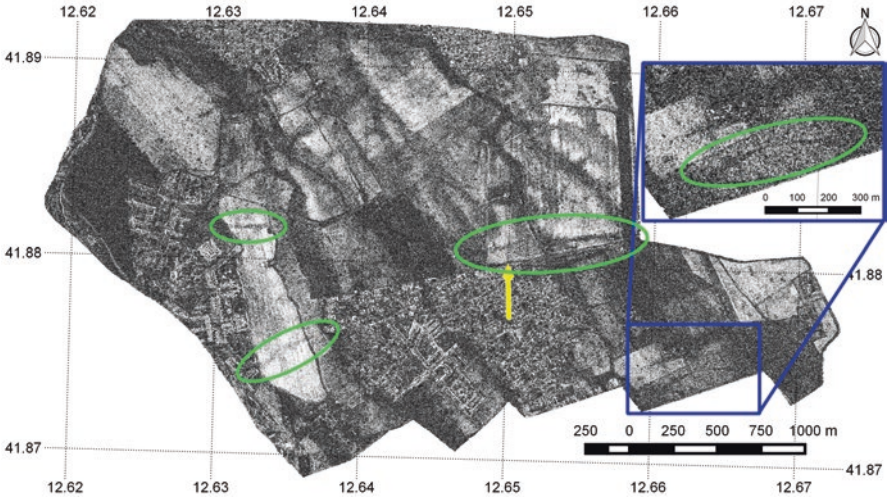

Fig. 10 Coherence image from CSK spotlight InSAR pair acquired on 9 and 25 July 2010 over the Prenestina AOI. Green ellipses show the locations of residues. The yellow arrow shows the location and direction from which the photo in Fig. 12 was acquired on the ground. COSMO-SkyMed data provided by the Italian Space Agency

Only some of the coherence residues correspond with faint backscatter traces, apart from one feature (see inset of Fig. 10), which clearly corresponds with a backscatter residue (see Figs. 7 and 8). Aside from this last feature, all correspond with clear topographic traces on the SBAS DEM (see Figs. 11 and 13).

DEM

An attempt at deriving heights using the SBAS technique only worked well for the Prenestina AOI. Over all other AOIs, the coherence was too low for most of the interferograms for the technique to work. The topographic features on the Prenestina AOI correspond with the location of ancient roads documented by Quilici (1974) (see Figs. 13 and 14). The scale of the topographic traces range from 50 m to 145 m in width and were all around 2 m in height.

Over the Prenestina AOI, while most of the interferograms had too low coherence, a very coarse DEM was possible from the image pair acquired on 10 and 26 August 2012 (see Fig. 15). The DEM is very noisy given the low coherence, but the ancient Via Salaria can be seen very clearly as a valley or ditch traversing the fields. This corresponds with the filtered backscatter residue (see Fig. 9), but interestingly, no obvious topographic trace is visible on the ground (see Fig. 9).

The image pair used for the DEM is not amongst those that reveal residues of the Via Salaria as backscatter anomalies. The presence of this slight valley may be the reason why the backscatter residue appears more clearly at a time of low PSMD,

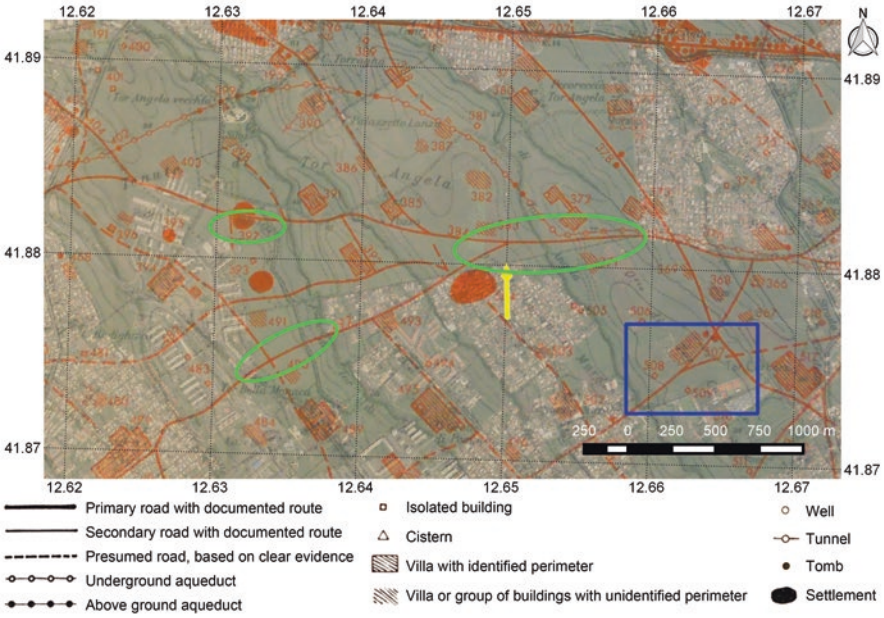

Fig. 11 Subset of archaeological chart over the Prenestina AOI published by Quilici (1974) as part of the Forma Italiae series. Red features show documented archaeological structures. Green ellipses and blue rectangle show the locations of residues visible in Fig. 10. The yellow arrow shows the location and direction from which the photo in Fig. 12 was acquired on the ground

Fig. 12 Photo acquired of one of the residues shown in Fig. 10. The photo shows that this residue is situated in the centre of a broad valley. The photo was acquired on 6 October 2015 at 12:36

as this would perhaps enhance the difference between abundant vegetation growth in the valley and stunted growth over the buried road.

The DEM image acquisitions coincide with high PSMD and high coherence. Perhaps shorter and dryer vegetation is less likely to contribute to temporal decorrelation than if the vegetation were healthy and abundant. Crop marks typically

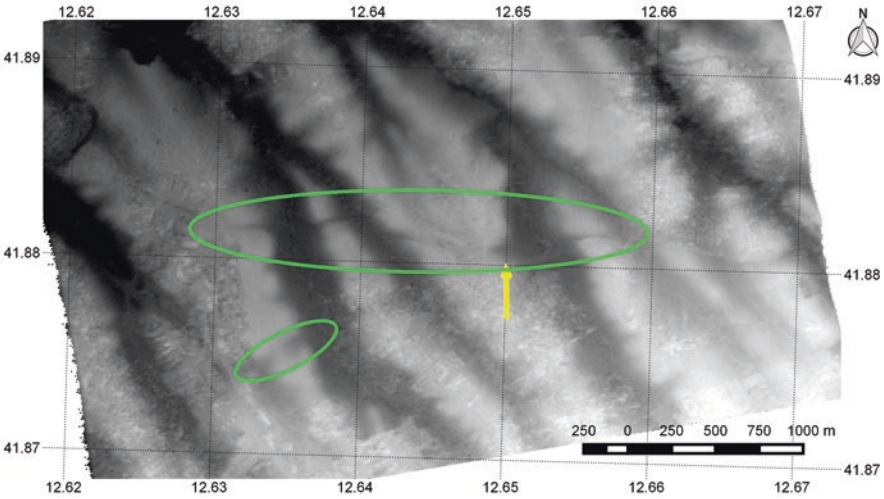

Fig. 13 SBAS DEM produced from CSK stripmap imagery over the Prenestina AOI. Green ellipses show the locations of archaeological features. Yellow arrow shows the location and direction from which the photo in Fig. 12 was acquired. COSMO-SkyMed data provided by the Italian Space Agency

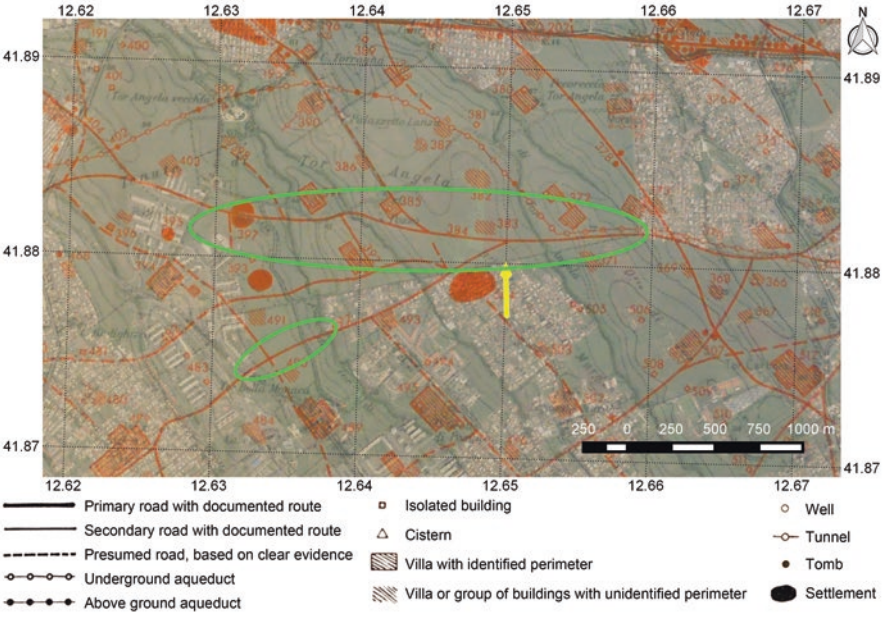

Fig. 14 Subset of archaeological chart over the Prenestina AOI published by Quilici (1974) as part of the Forma Italiae series. Annotations in red show documented archaeological structures. Green ellipses show the locations of residues. Yellow arrow shows the location and direction from which the photo in Fig. 12 was acquired

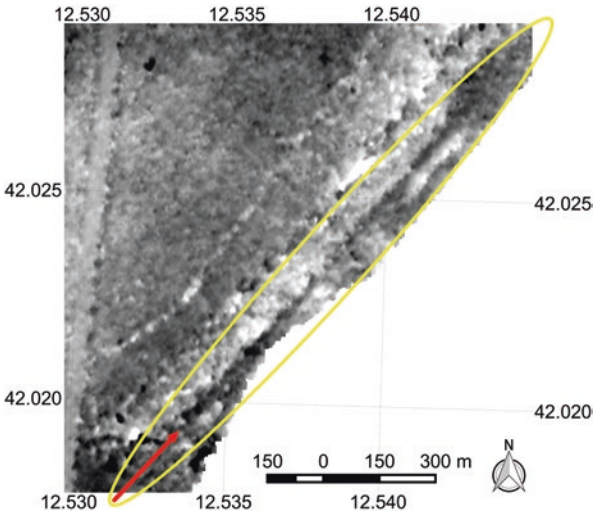

Fig. 15 DEM over the Salaria AOI derived from InSAR using the CSK stripmap image pair acquired on 10 and 26 August 2012. Yellow ellipse shows location of the residue of the ancient Via Salaria. The DEM is very noisy, but the residue of the ancient Via Salaria can clearly be seen. Red arrow shows the direction and location from which the photo in Fig. 9 was acquired

emerge in such conditions when plants are in need of moisture (Jones and Evans 1975; Evans and Jones 1977; Agapiou et al. 2013). It may be therefore that the topographic anomaly is due to differential crop growth, perhaps not as enhanced as at other times but possible to measure with InSAR due to the higher coherence.

Conclusions

This study demonstrates that surface residues of buried archaeological features in temperate vegetated areas can (in some cases) be detected in SAR data. It also shows that full use of all information contained in both the amplitude and phase of SAR data can greatly enhance the detection capability. The study reveals that some archaeological features are better visible as one of either coherence, topographic or backscatter residues. Analysing all three not only helps to detect features, but it also helps to interpret them as either soil marks or as positive or negative crop marks, which in turn provides more information on the structure buried beneath the ground.

The study also demonstrates how a large time series of data can greatly aid detection of features. The more data is available, the better the speckle can be removed through filtering in the temporal domain, to preserve spatial resolution. A large time series also improves the ability to produce a DEM in vegetated areas using the SBAS technique. Finally, with a coherence time series, additional information on the state of the vegetation cover can be derived, which can aid interpretation of features.

SAR in Desert Areas

The sensitivity of SAR to roughness and relative permittivity renders it very useful in desert environments. Under certain conditions, microwave radiation can penetrate into dry sand. The penetration depth, δ_P, is a function of the microwave wavelength, λ, and the relative permittivity, $\varepsilon = \varepsilon' - j\varepsilon''$, according to the expression

$$\delta_P \cong \frac{\lambda\sqrt{\varepsilon'}}{2\pi\varepsilon''} \tag{1}$$

This is valid when $\varepsilon''/\varepsilon' < 0.1$, which is the case for most natural land surfaces, including sand (Ulaby et al. 1982).

For dry sand, the imaginary component of the relative permittivity is very low, which explains why signal penetration occurs at microwave wavelengths. The expression also shows that the longer the wavelength, the greater the penetration.

The real interest in the use of SAR remote sensing for geoarchaeological applications followed the Shuttle Imaging Radar (SIR-A) discovery of buried palaeorivers in the Sahara in November 1981. The imagery acquired over the Selima Sand Sheet, and drift sand of the eastern Sahara, revealed previously unknown buried valleys and geologic features (McCauley et al. 1982). SIR-A operated at L-band wavelength (24 cm), but even shorter wavelengths can reveal features beneath a layer of sand due to signal penetration. Figure 16 shows a part of the area first imaged by SIR-A, revisited with Sentinel-1 and Sentinel-2. Even at the shorter frequency of C-band, the palaeorivers of the Bir Safsaf area of the Eastern Sahara are clearly visible in the Sentinel-1 data, while the Sentinel-2 data provides information on the surface characteristics.

A recent study is summarised here on the systematic extraction of anthropogenic features in the North Sinai desert, taking advantage of the unique characteristics of microwave interaction with dry sand. To fully exploit these characteristics, both the amplitude and phase of long-wavelength SAR data from the phased array type L-band SAR (PALSAR) sensor have been used. A full description of the research is described in Stewart et al. (2016).

The North Sinai desert was chosen as a test area due to its archaeological importance as a land bridge connecting Africa and Western Asia (e.g. Mumford (2015) and Oren (1989)). The area is composed mainly of Aeolian sand dune fields and interdune areas, referred to as the northern Sinai dune field, or the Sinai-Negev erg (Muhs et al. 2013). A significant problem in the region is caused by sand drift and dune migration, which can rapidly bury ancient sites that may have been excavated in the past (Di Iorio et al. 2010), and even modern structures (Misak and Draz 1997; Hermas et al. 2012). The large size of the region, combined with the inhospitable terrain and frequent political instability (Gold 2014), makes regular systematic survey of the area challenging. Efficient and cost-effective methods for regular, large-scale surveys of such areas are therefore very much required. This area was chosen as a test site to determine whether SAR remote sensing techniques could meet these requirements (see Fig. 17).

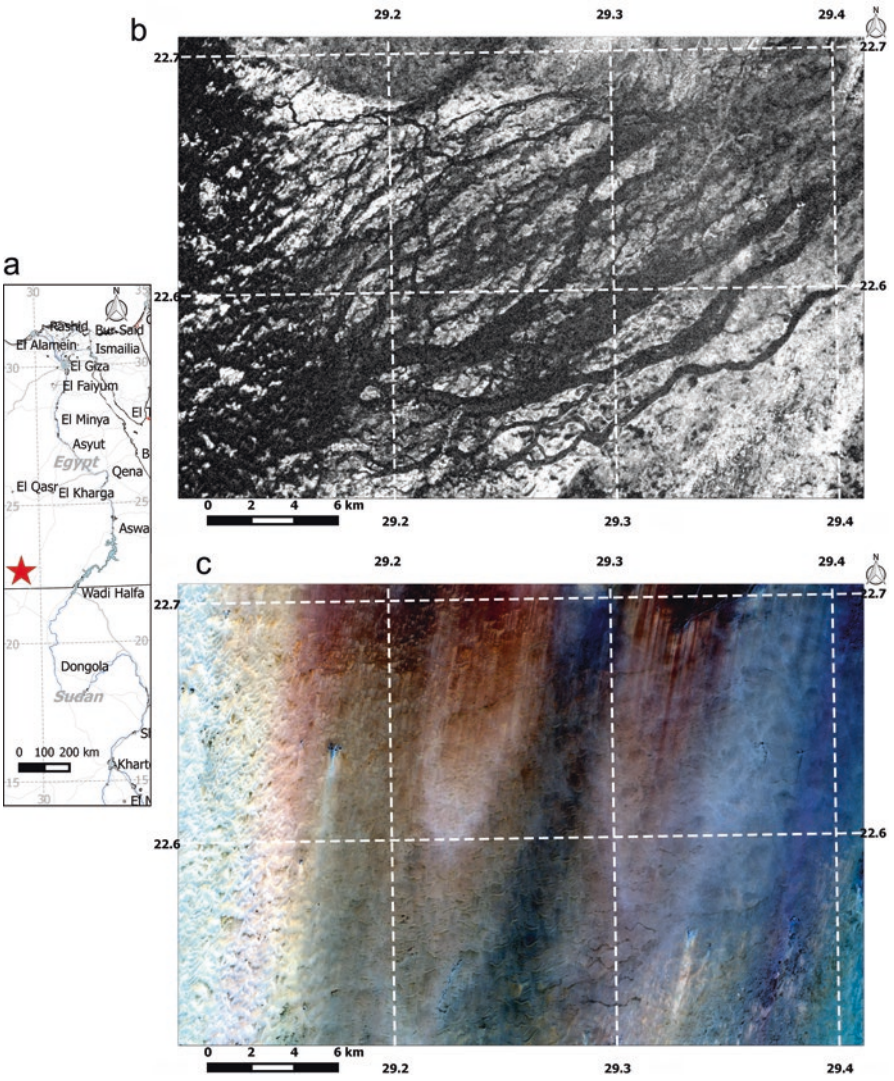

Fig. 16 (**a**) Map of the Bir Safsaf area where the images in (**b**) and (**c**) were acquired. (**b**) Sentinel-1A IW GRD VV σ^0 backscatter (in dB) image acquired on 11 February 2016. (**c**) Sentinel-2A L1C image acquired on 20 March 2016 corresponding to the same area as in (**b**). Displayed as a true-colour combination of band 4 (red), band 3 (green) and band 2 (blue). Contains modified Copernicus Sentinel data 2017

Table 2 shows the characteristics of the SAR data used for the analysis. Seventy-four PALSAR-1 images in fine beam single and fine beam dual polarisation modes were obtained from the European Space Agency (ESA). These were acquired over nine tracks and frames which together almost completely cover the North Sinai desert (see Fig. 17). For each track and frame, a time series of (on average seven) images was available with a date range from 2007 to 2010 or 2011. Over a small subset area,

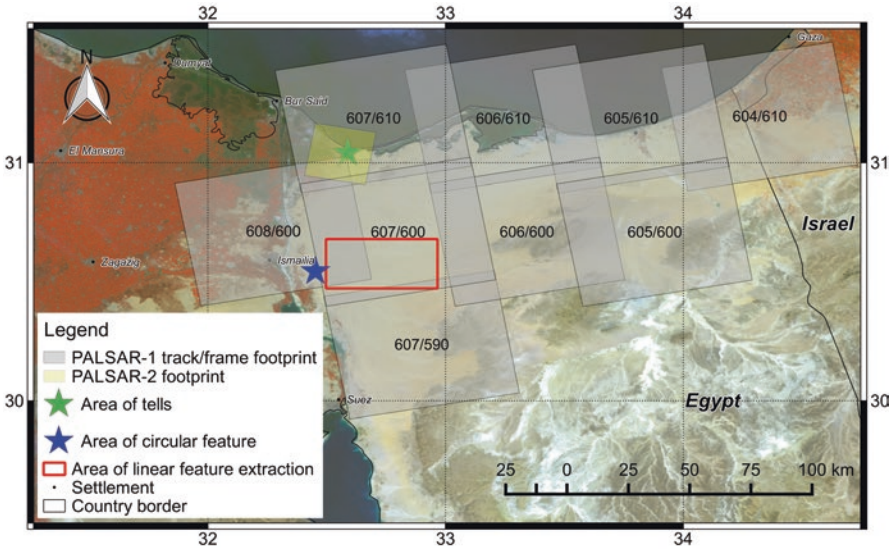

Fig. 17 Map showing North Sinai with the footprints of the PALSAR-1 and 2 imagery used for the analysis. The track/frame identification number of each PALSAR-1 stack is shown. The locations of features and areas of interest are shown by green and blue stars and red rectangle. The background image is a near-infrared and visible false-colour composite of an ENVISAT Medium-Resolution Imaging Spectrometer (MERIS) image at 300 m resolution with band 10 (754 nm) displayed as red, band 5 (560 nm) as green and band 2 (443 nm) as blue. Data provided by ESA

Table 2 Characteristics of PALSAR-1 and 2 imagery used for the analysis

Sensor	PALSAR-1	PALSAR-2
Number of scenes	74	7
Acquisition date range (year/month)	2007/06 to 2011/02	2015/08 to 2015/10
Polarisation	HH	HH
Pass	Asc	Des
Scene centre incidence angle	38.7	40–49
Final pixel spacing	10 m	2 m
Wavelength	23.6 cm (L-band)	22.9 cm (L-band)

new acquisitions of PALSAR-2 data in spotlight mode were requested to the Japanese Space Agency (JAXA), who provided seven new data acquisitions in 2015.

The objective of the analysis and the chosen dataset was to experiment with different techniques for anthropogenic feature detection over multiple areas and make full use of the information content of the time series. Techniques were applied on both the amplitude and the phase of the data in single-look complex (SLC) format. With the amplitude data, multitemporal De Grandi speckle filtering was applied to reduce the image speckle while preserving spatial resolution. Time series analysis was carried out to determine the utility of the mean, maximum, minimum, standard deviation and other parameters calculated from the time series. Processing of the

phase involved coherence calculation between consecutive image acquisitions and averaging all coherences.

An analysis of all imagery was carried out by a multidisciplinary team of Egyptologists, geologists and SAR experts. A comparison of the SAR-derived information was also made with other raster and vector information layers in a geographic information system (GIS). These layers included geological and archaeological charts, remotely sensed optical imagery and web map service (WMS) vector layers of infrastructure (roads, railways, canals, etc.). The objective of this analysis was to assess whether any potential anthropogenic features existed which were uniquely identified, or better highlighted, in the variously processed SAR data.

Results of this analysis revealed that many seemingly man-made features were distinguished by abnormally high backscatter compared to the surrounding sand. Many of these were in linear form. A much smaller number of potential anthropogenic structures were characterised by lower backscatter relative to surrounding areas. These were mainly confined to an area near the eastern Nile delta and Mediterranean coast, around the archaeological sites of Tell el-Farama, Tell el-Mahzan and Tell el-Kanais (see Fig. 17). It was decided to focus further research on two areas of interest (AOIs):

AOI 1. The region east of Ismailia: An area of mobile sand dunes where many anomaly linear features of high relative backscatter were identified.
AOI 2. The area of Tell el-Farama, Tell el-Mahzan and Tell el-Kanais: A coastal area with potential archaeological features of low relative backscatter.

Over AOI 1, many of the features of high backscatter that seemed likely to be anthropogenic were of a linear nature. A method was attempted to extract these and convert them to vector format to facilitate comparison and analysis with other layers in the GIS. A linear feature detection algorithm was thus developed. This was first attempted using the multitemporal De Grandi speckle filtered imagery as input. It worked by performing the following tests, for straight lines in all orientations, in a moving window of pixels:

$$\text{a.} \quad \bar{x}_L > T_1 * \bar{x}_B \tag{2}$$

$$\text{b.} \quad \sigma_L > T_2 * \sigma_B \tag{3}$$

$$\text{c.} \quad \sigma^2\left(\theta_{\text{LOCAL}}\right) < T_3 \tag{4}$$

where, for a line of a particular orientation, $\bar{x}_L$ is the mean value of pixels along the line, $\bar{x}_B$ is the mean value of background pixels (outside the line, but within the moving window of pixels), σ_L is the standard deviation of line pixels, σ_B is the standard deviation of pixels outside the line, $\sigma^2(\theta_{\text{LOCAL}})$ is the variance of the local incidence angle (calculated from the SRTM 1 arc-second DEM) and T_1, T_2 and T_3 are threshold values.

Test c was necessary to discard lines caused by high backscatter from sand dunes. At small incidence angles, peak backscatter usually occurs at the incidence angle equal to the angle of repose of sand dunes (Blom and Elachi 1987). Particularly for sand dunes oriented along the SAR azimuth direction, a line of bright pixels can be seen along the dunes.

It was noticed that the average coherence revealed the same pattern of high-backscatter features (but as areas of high coherence) but without the lines over the sand dunes. The linear feature extraction algorithm was therefore applied using the average coherence as input and discarding test c. This yielded much better results.

Over AOI 2, a time series of PALSAR-2 spotlight imagery was procured to complement the existing data. Processing included a range of multitemporal techniques to better extract the low-backscatter anomaly structures. These were then interpreted through comparison with other information layers and with the results of previous archaeological survey in the area.

Results

High-Backscatter Features

An example of a seemingly man-made feature of high backscatter is shown in Fig. 18. This is one of the many features identified by the team of geologists, archaeologists and remote sensing experts that do not appear in any of the available optical remote sensing imagery or WMS data. The concentric circles shown in Fig. 18 are present in all the seven De Grandi speckle filtered PALSAR-1 images in the time series acquired over this area from November 2007 to April 2010. As shown in the

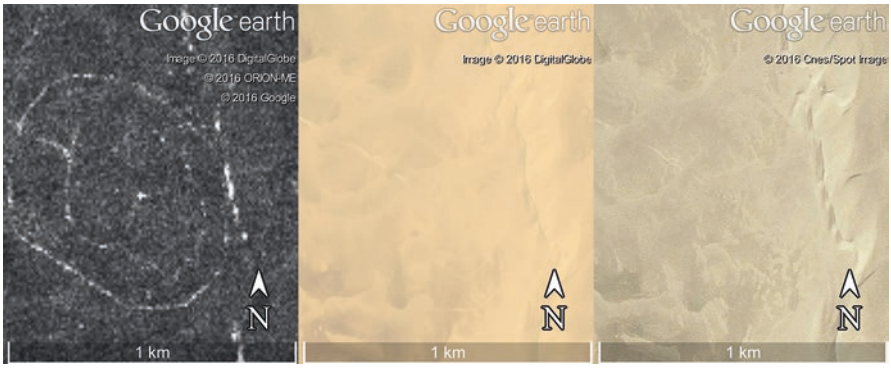

Fig. 18 Left: Feature identified in PALSAR-1 De Grandi filtered backscatter imagery. The feature is centred at 30.544° latitude and 32.452° longitude. Centre: Optical image of the same area, available on Google Earth, acquired on 5 May 2010. Right: Optical image of same area, available on Google Earth, acquired on 7 February 2007. PALSAR-1 data provided by ESA

figure, the same features are not evident in the two very-high-resolution (VHR) optical images available on Google Earth, reported, respectively, in February 2007 and May 2010. While the shape of this feature may resemble that of early Bronze Age sites, such as those illustrated in Arieh (1974), its scale does not. The feature in the SAR imagery is around one order of magnitude larger than the early Bronze Age sites in Arieh (1974). It is more likely that this particular feature is a buried relic of a military installation from one of the past wars that took place in this region, such as the Six Day War (Dunstan 2012).

Over AOI 1, results of the linear feature extraction algorithm applied to the average coherence image are shown in Fig. 19. Figure 19a shows a Sentinel-2 optical image of the AOI overlain with all available vectors of infrastructure which appear on at least one of the following WMS: Google Maps, Open Street Map, Bing Maps and Apple iPhoto map. Figure 19b shows the same Sentinel-2 image overlain with the vectors of anthropogenic linear features extracted automatically from the average

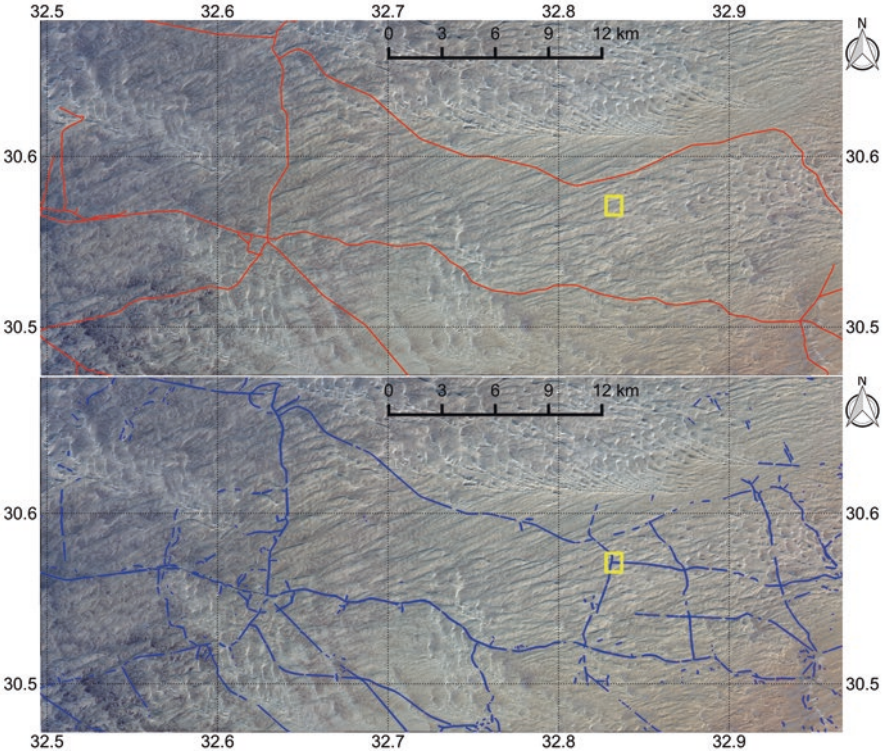

Fig. 19 Top: Sentinel-2 image over AOI 1 overlain with all WMS vectors of infrastructure (in red) from Google Maps, Open Street Map, Bing Maps and Apple iPhoto map. Image acquired on 19 February 2016. Full-resolution (10 m) true-colour composite. All vectors correspond to roads. Bottom: Lines extracted from average PALSAR-1 coherence (in blue) overlain on the same Sentinel-2 subset image as in top part of figure. Yellow rectangle shows location of detail in Fig. 20. Contains modified Copernicus Sentinel data 2016

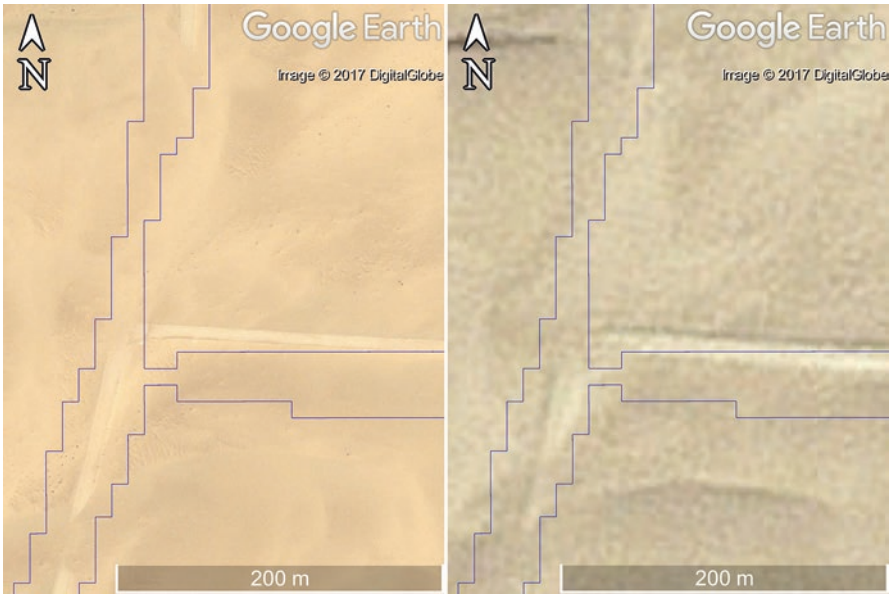

Fig. 20 Detail of partially buried road junction on optical remotely sensed images available on Google Earth acquired on 5 May 2010 (left) and 7 February 2007 (right). Lines extracted from average PALSAR-1 coherence overlain in blue. The road junction is an example of a feature not present on any of the available WSM vector layers. It appears unchanged from 2007 to 2010 and is visible in multitemporal speckle filtered PALSAR-1 imagery also from 2007 to 2010

coherence image. Many linear features extracted from the SAR data are not present in any of the considered WMS vectors. Figure 20 shows a close-up of an area containing such features overlain on VHR optical imagery available on Google Earth, purported to have been acquired on 7 February 2007 and 5 May 2010, respectively. In both images traces of partially buried tracks correspond with the SAR-derived vectors overlain. The pattern of sand dunes in both images seems the same and suggests that no significant sand dune movement took place between the two acquisition dates.

Low-Backscatter Features

Over AOI 2, the features of potential archaeological interest characterised by low backscatter are evident in Fig. 21. This shows the areas surrounding Tell el-Farama, Tell el-Mahzan and Tell el-Kanais in the average of De Grandi filtered PALSAR-1 images in Fig. 21a, and a close-up of the areas of Tell el-Mahzan and Tell el-Kanais in the coefficient of variation (CoV) of the De Grandi filtered PALSAR-2 spotlight images in Fig. 21b. Figure 22 shows the same area and close-up detail as in Fig. 21, on a VHR optical satellite image acquired by the Pleiades sensor.

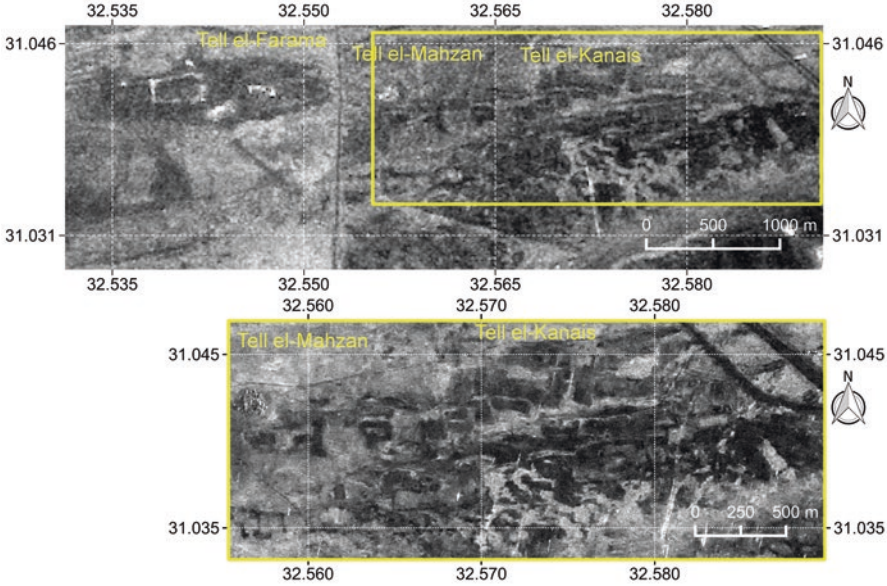

Fig. 21 Top: Average of De Grandi filtered PALSAR-1 images over the region of tells in AOI 1 (Tell el-Farama, Tell el-Mahzan and Tell el-Kanais). Yellow rectangle shows area of bottom part of figure. Data provided by ESA. Bottom: Coefficient of variation of seven PALSAR-2 spotlight multitemporal De Grandi speckle filtered images over the region surrounding Tell el-Mahzan and Tell el-Kanais. PALSAR-2 data provided by JAXA

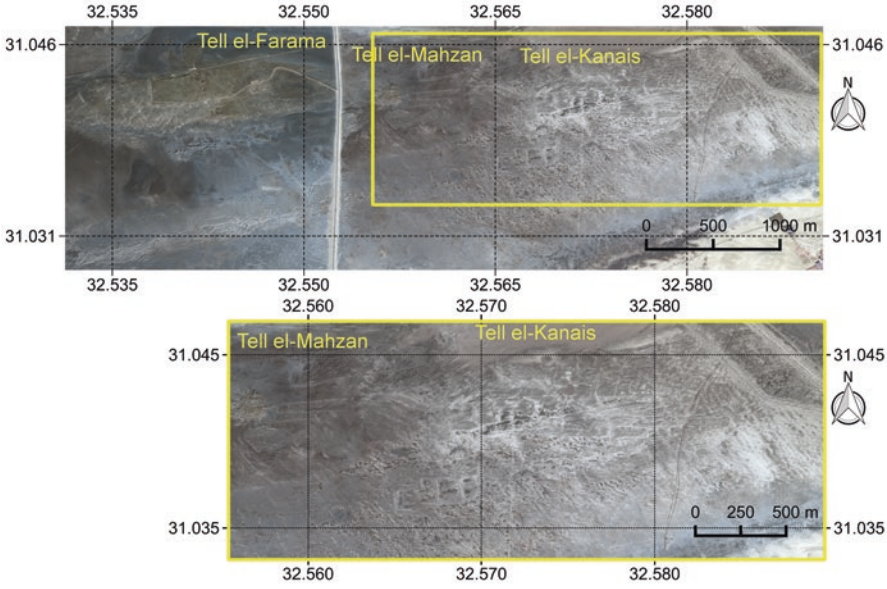

Fig. 22 Pleiades image acquired on 24 November 2015, covering the same area as in Fig. 21. Image has been pansharpened to 0.5 m pixel spacing and is displayed as enhanced true-colour composite. Pleiades data provided by ESA

The tells were thriving inhabited areas when the Pelusiac branch of the Nile was active and when the Mediterranean coastline was situated just to the north of the tells. Its importance declined when the coastline migrated north and the Pelusiac Branch silted up and was eventually abandoned by the time of the Crusades (Stanley et al. 2008). The area comprises silt and sand, covered in places with salt crusts (Jaritz et al. 1996).

For the areas of Tell el-Mahzan and Tell el-Kanais, Jaritz and his colleagues published a map showing the distribution of anthropogenic surface remains in four density classes. The map shows that surface remains seem to be clustered in a number of islands (Jaritz et al. 1996). It was suggested by the authors of this map that these islands may have been dry areas, more attractive for settlement, surrounded by wet and marshy land. Interestingly, the dark features on both the PALSAR-1 and 2 data show a similar pattern of island features, characterised by lower backscatter and lower CoV of backscatter. It is suggested by Stewart et al. (2016) that a possible reason why this pattern is also visible in the SAR data is that there may still be a higher concentration of moisture in the formerly inundated areas. This increased moisture presence would likely produce a higher SAR backscatter response given the increased relative permittivity (Ulaby et al. 1982).

Conclusions

The sensitivity of SAR to surface roughness and the relative permittivity of materials have long been recognised as useful for archaeological applications in desert regions. The recent study carried out by Stewart et al. (2016) demonstrates the added value that can be derived from using the phase in addition to the amplitude of SAR data for feature extraction in desert regions. It also shows the utility of having a time series.

Analyses of long-wave PALSAR-1 and 2 data over the North Sinai desert show that features of historical interest can be efficiently identified and extracted over large areas. These features may be characterised by high backscatter and high coherence relative to surrounding areas, or by low backscatter. An interpretation of such features can be challenging and is often not possible using the SAR data alone.

In the case of the high-backscatter features, an automatic extraction algorithm was devised to detect only linear anthropogenic structures. It was discovered that a distinction between backscatter due to natural sand dunes and anthropogenic features could be more efficiently carried out with images of average coherence rather than backscatter intensity. However, in either case, no distinction was made between ancient and modern features. Nonetheless, efficient techniques to detect human infrastructure (modern or ancient) abandoned or partially covered by sand could be of significant utility in North Sinai given the problems associated with sand drift and dune migration in the region, which can rapidly bury modern structures (Misak and Draz 1997; Hermas et al. 2012) or ancient sites that may have been excavated in the past (Di Iorio et al. 2010).

In a coastal region of the eastern Nile delta, a number of low-backscatter features were evident in the areas of Tell el-Farama, Tell el-Mahzan and Tell el-Kanais. A possible interpretation of these was suggested by Stewart et al. (2016) following the comparison of SAR-derived results with the outcome of previous research in the region. Identification of features in the SAR data was aided by the availability of not just one but a time series of SAR imagery. This enabled speckle reduction and the extraction of parameters such as the coefficient of variation, in which features of potential archaeological interest were more evident. Identification of features was also facilitated by the availability of higher resolution data in the form of a time series of PALSAR-2 spotlight imagery.

Discussion

Microwaves interact uniquely with surface materials. Recent studies present novel ways that this interaction can be exploited for archaeological applications over land cover types typical to Europe (such as areas of bare soil, crop and grassland) and the Middle East (such as desert sand and coastal mudflat). These attempt to exploit the full information content of SAR data, contained in both the amplitude and phase of the signal. They also attempt to make efficient use of time series.

These studies have been carried out at a time of unprecedented increase in the quantity and availability of data which is stimulating a complete transformation in scientific analysis and operational usage. Previous limitations on data volume, costs, analysis time and complexity are progressively being overcome, and we are seeing the potential for new applications and user communities to reap the benefits. The complexity of SAR data processing and interpretation has always been challenging and has hindered its uptake in many application areas, including cultural heritage. Demonstrations of the successful utility of SAR for cultural heritage managers could help to raise awareness of its benefits and accelerate its eventual adoption as an operational tool.

References

Agapiou A, Hadjimitsis DG, Sarris A, Georgopoulos A, Alexakis DD (2013) Optimum temporal and spectral window for monitoring crop marks over archaeological remains in the Mediterranean region. J Archaeol Sci 40(3):1479–1492

Arieh IB (1974) An early Bronze Age II site at Nabi Salah in southern Sinai. Tel Aviv 1(4): 144–156

Berardino P, Fornaro G, Lanari R, Sansosti E (2002) A new algorithm for surface deformation monitoring based on small baseline differential SAR interferograms. IEEE Trans Geosci Remote Sens 40(11):2375–2383

Blom R, Elachi C (1987) Multifrequency and multipolarization radar scatterometry of sand dunes and comparison with spaceborne and airborne radar images. J Geophys Res B 92(B8):7877–7889

De Grandi GF, Leysen M, Lee JS, Schuler D (1997) Radar reflectivity estimation using multiple SAR scenes of the same target: technique and applications. In: Geoscience and remote sensing, 1997. IGARSS'97. Remote sensing-a scientific vision for sustainable development, 1997 IEEE International, vol 2. IEEE

Di Iorio A, Straccia N Carlucci R (2010) Advancement in automatic monitoring and detection of archaeological sites using a hybrid process of remote sensing, GIS techniques and a shape detection algorithm. In: Proceedings of the 30th EARSeL Symposium, Paris, vol 31, pp 53–63. Paris

Dubois PC, Van Zyl J, Engman T (1995) Measuring soil moisture with imaging radars. IEEE Trans Geosci Remote Sens 33(4):915–926

Dunstan S (2012) The six day war 1967. Bloomsbury Publishing, Sinai

Evans R, Jones RJ (1977) Crop marks and soils at two archaeological sites in Britain. J Archaeol Sci 4(1):63–76

Gold Z (2014) Security in the Sinai: present and future. ICCT Research Paper, March

Hermas E, Leprince S, El-Magd IA (2012) Retrieving sand dune movements using sub-pixel correlation of multi-temporal optical remote sensing imagery, northwest Sinai Peninsula, Egypt. Remote Sens Environ 121:51–60

Jaritz H, Favre S, Nogara G, Rodziewicz M, Carrez-Maratray J-Y (1996) Pelusium. prospection archéologique et topographique de la région de Tell el-Kana'is 1993 et 1994. Beiträge zur ägyptischen Bauforschung und Altertumskunde 12:29

Jones RJ, Evans R (1975) Soil and crop marks in the recognition of archaeological sites by air photography. Aerial Reconnaissance Archaeol:1–11

Keay S, Millett M, Paroli L, Strutt K (2005) Portus: an archaeological survey of the port of Imperial Rome, vol 15. British School at Rome, London

Manyika J, Chui M, Brown B, Bughin J, Dobbs R, Roxburgh C, Byers AH (2011) Big data: the next frontier for innovation, competition, and productivity. McKinsey, Lexington

Massonnet D, Souyris J-C (2008) Imaging with synthetic aperture radar. CRC Press, Boca Raton

McCauley JF, Schaber GG, Breed CS, Grolier MJ, Haynes CV, Issawi B et al (1982) Subsurface valleys and geoarcheology of the eastern Sahara revealed by shuttle radar. Science 218(4576):1004–1020

Misak R, Draz M (1997) Sand drift control of selected coastal and desert dunes in Egypt: case studies. J Arid Environ 35(1):17–28

Muhs DR, Roskin J, Tsoar H, Skipp G, Budahn JR, Sneh A et al (2013) Origin of the Sinai–Negev erg, Egypt and Israel: mineralogical and geochemical evidence for the importance of the Nile and sea level history. Quat Sci Rev 69:28–48

Mumford G (2015) The Sinai Peninsula and its environs: our changing perceptions of a pivotal land bridge between Egypt, the Levant, and Arabia. J Anc Egypt Interconn 7(1):1–24

Oren ED (1989) Early Bronze Age settlement on northern Sinai: a model for Egypto-Canaanite interconnections. In: de Miroschedji P, L'urbanisation de la Palestine à l'âge du Bronze ancien. Bilan et perspectives des recherches actuelles. Actes du Colloque d'Emmaüs (20–24 octobre 1986), vol 527. Oxford: BAR IS, pp 389–405

Quilici L (1974) Collatia (Vol. Regio 1). De Luca Editore, Rome

Stanley J-D, Bernasconi MP, Jorstad TF (2008) Pelusium, an ancient port fortress on Egypt's Nile Delta coast: its evolving environmental setting from foundation to demise. J Coast Res:451–462

Stewart C (2017) Detection of archaeological residues in vegetated areas using satellite synthetic aperture radar. Remote Sens 9(2):45

Stewart C, Montanaro R, Sala M, Riccardi P (2016) Feature extraction in the north Sinai desert using spaceborne synthetic aperture radar: potential archaeological applications. Remote Sens 8(10):27

Ulaby T, Moore K, Fung K (1982) Microwave remote sensing. Volume II: radar remote sensing and surface scattering and emission theory. Addison Wesley, New York

Wilson DR (2000) Air photo interpretation for archaeologists. Tempus Publishing, Stroud

Wiseman J, El-Baz F (2007) Remote sensing in archaeology. Interdisciplinary contributions to archaeology. Springer, New York

Zalite K, Voormansik K, Praks J, Antropov O, Noorma M (2014) Towards detecting mowing of agricultural grasslands from multi-temporal COSMO-SkyMed data. In: Proceedings of the 2014 IEEE geoscience and remote sensing symposium. Quebec City: IEEE, pp 5076–5079

Zalite K, Antropov O, Praks J, Voormansik K, Noorma M (2016) Monitoring of agricultural grasslands with time series of X-band repeat-pass interferometric SAR. IEEE J Sel Top Appl Earth Observ Remote Sens:3687–3697